



CrossMark
 click for updates

Cite this: *RSC Adv.*, 2015, 5, 66549

Received 17th June 2015
 Accepted 28th July 2015

DOI: 10.1039/c5ra11614g

www.rsc.org/advances

Selective protein purification by PEG–IDA-functionalized iron oxide nanoparticles†

M. Bloemen,^{‡*a} L. Vanpraet,^{‡a} M. Ceulemans,^b T. N. Parac-Vogt,^b K. Clays,^a
 N. Geukens,^c A. Gils^d and T. Verbiest^a

We developed a new heterobifunctional polyethylene glycol ligand for iron oxide nanoparticles with a group for covalent surface attachment and for chelating metal ions. After introduction of nickel ions, His-tagged fluorescent proteins were magnetically purified from a cell lysate. A high purity product and efficient magnetic separation were observed.

Introduction

Superparamagnetic nanoparticles have attracted a lot of attention thanks to their applicability and unique properties. Iron oxide particles (such as magnetite) are frequently used in hyperthermia, magnetic resonance imaging, optical or drug carrier experiments.^{1–7} They have a unique magnetic behavior called superparamagnetism, which is the absence of a net magnetic moment without an applied magnetic field (similar to a paramagnet), while having a magnetic susceptibility comparable to a ferromagnetic material.⁴ This largely facilitates their handling during functionalization procedures, while they still retain a high saturation magnetization, which enables a fast magnetic separation.^{8,9}

Many synthetic procedures have been reported to produce these nanoparticles with different shapes and sizes.^{10–14} One of the more popular methods uses an organic iron precursor in a thermal decomposition process, as reported by Park *et al.*¹¹ It is known to produce well defined, spherical and monodisperse

nanoparticles with a size between 7 and 22 nm. Their surface is covered with apolar oleic acid ligands, which have to be replaced for applications in aqueous environments. A so-called ligand exchange process can be performed to introduce new organic molecules, polymers or a silica shell onto the surface.^{15–18}

The long-standing standard technique for protein purification with a polyhistidine tag employs beaded agarose packed in a column, with nitrotriacetic acid to immobilize the nickel. While a tried-and-true method; lengthy wash steps and limited flow speeds are required due to the permanently packed column configuration.^{19,20} This also limits the possibilities in terms of parallel high-throughput purification. Furthermore, the highly specialized nature and complexity in production of appropriate agarose beads results in high material costs.

In contrast to this, functionalized nanoparticles are straightforward and cheap to produce. Their magnetic nature allows easy and rapid suspension and recapture throughout the purification process. This flexibility severely reduces wash times and opens up new possibilities in terms of parallel purification and automation.

The use of a fluorescent protein during the purification tests provided a direct visual feedback throughout the experiments. The comparison of color intensity between repeated experiments provided direct information in terms of success and repeatability of the experiments.

DsRed is a tetrameric red fluorescent protein with an excitation and emission maximum at 558 nm and 583 nm, respectively.²¹ It was selected as a model for these experiments for two distinct reasons. Firstly, its absorption maximum at longer wavelengths allows determining the protein concentration, without interference from stray nanoparticles. Secondly, its obligate tetrameric nature would test any issues with the elution capability. Since the imidazole moieties of the His-tag bind readily to the charged nickel, the binding of the protein to the nanoparticles would not be an issue. Proper elution is however more challenging. The tetrameric nature of the protein implies that the purified protein would have four His-tags,

^aKU Leuven, Department of Chemistry, Celestijnenlaan 200D, box 2425, 3001 Heverlee, Belgium. E-mail: maarten.bloemen@fys.kuleuven.be; Tel: +32 16 328251

^bKU Leuven, Department of Chemistry, Celestijnenlaan 200F, box 2404, 3001 Heverlee, Belgium

^cPharmAbs, The KU Leuven Antibody Center, KU Leuven, O&N II, Herestraat 49, box 820, 3000 Leuven, Belgium

^dKU Leuven, Department of Pharmaceutical and Pharmacological Sciences, O&N II, Herestraat 49, box 820, 3000 Leuven, Belgium

† Electronic supplementary information (ESI) available. See DOI: 10.1039/c5ra11614g

‡ These authors contributed equally.

resulting in a stronger bond to the nanoparticles, which in turn would reveal any problems with their separation during elution.

In this manuscript we developed a new heterobifunctional siloxane–polyethylene glycol ligand that can couple covalently to the surface of iron oxide nanoparticles, and has one imino diacetic acid (IDA) group at the end. The covalent linkage to the surface is crucial for ensuring a stable coating, which will not be removed at extreme pH or ionic strength. Thanks to the polyethylene glycol (PEG) chain, the colloidal stability of the particle is improved and becomes less dependent on the overall charge.²³ The IDA group at the end is capable of forming a stable complex with Ni(II) ions, which are subsequently capable of interacting with polyhistidine tags. Combined with the magnetic behavior of the core material, this forms a highly efficient tool for magnetic separations. Recently reported purification procedures of His-tagged proteins make use of very large micrometer-sized particles, very complex ligands or require several synthetic steps on the particle itself.^{24–30} Sahu *et al.* reported a surface modification with *N*-phosphonomethyl iminodiacetic acid that is capable of forming nickel complexes.²⁹ Another popular method is the preparation of TiO₂ mesoporous structures, in which the targeted molecule fits perfectly.^{31,32} The nanoparticle-based (8 nanometer in diameter) approach presented here, has a surface to volume ratio that is 100 times larger than micro-particle systems and hence can capture more proteins. The proposed ligand is synthesized separately from the particles, which allows for a better characterization and possibly better yields. Moreover, the straightforward synthetic protocol, covalent bond with the surface and the rigorously tested proof of concept in a complex environment, will ensure a more rapid implementation into applications.

Results and discussion

To design the PEG ligand with specific nickel interactions, we chose to use iminodiacetic acid (IDA) instead of nitriloacetic acid (NTA) as the chelating group and work with siloxane chemistry to covalently attach it to the nanoparticle's surface. The choice for IDA is a tradeoff between the stability constant of the nickel complex (NTA > IDA) and the density of binding positions on the surface (IDA > NTA). Moreover the elution generally requires a lower concentration of imidazole, which might influence the colloidal stability of the nanoparticles.

By reacting ethanolamine with *tert*-butyl bromoacetate in a nucleophilic substitution reaction, the protected IDA molecule (**1**) was obtained (see Fig. 1). Secondly, its hydroxyl group was esterified with a carboxylic acid on a heterobifunctional PEG chain.³³ The PEG molecule was obtained by oxidizing allyl-PEG₁₀-OH with *in situ* produced chromic acid. This is one of the few appropriate methods that do not interfere with the allyl group. Potassium permanganate for instance would oxidize both groups.³⁴ By performing this reaction in acetone, the reduced chrome salts precipitate, which speeds up the reaction. Even though the deprotection of the IDA group could have been performed at this stage, we postponed it to after the surface functionalization reaction. This approach reduces the chance of wrongful orientation of the ligand (carboxylic acid can interact with iron atoms on the surface) and makes sure that only the siloxane will covalently link to the surface.³⁵ Moreover, the excess base during the functionalization procedure can charge free carboxylic acids and make the nanoparticle colloidal unstable (due to polarity).

The subsequent thiol–ene Click reaction is very convenient for introducing siloxane moieties, since it is fast, high yielding and with virtually no side products.^{36,37} Siloxanes have a

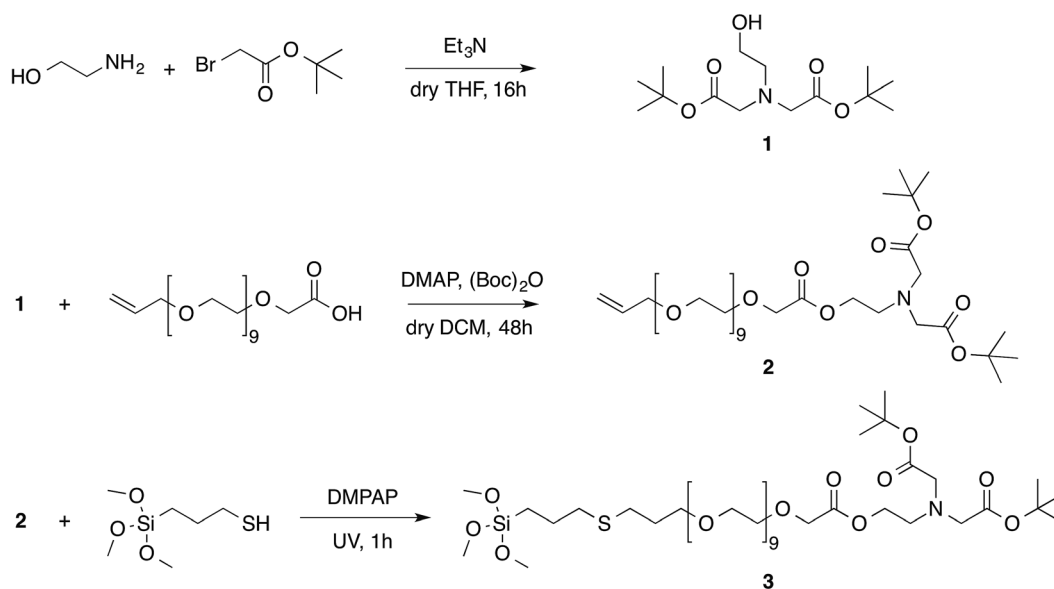


Fig. 1 The synthesis of the ligand starts with the formation of a functionalized ethanolamine molecule (**1**), which is later on attached to the PEG chain via an ester bond, to form the allyl-PEG–IDA–tBu molecule (**2**).²² Finally, a siloxane molecule is clicked to the allyl group of molecule **2**, by thiol–ene Click chemistry, resulting in the completed ligand (**3**).

tendency to crosslink in the presence water or prolonged exposure to heat. Therefore a fast reaction is required, with minimal heating involved. The absence of side products allowed us to use the synthesized ligand without further purification. Ligand 3 was mixed with the initial allyl-PEG molecule (ratio 10/90) during the Click reaction, resulting in a mixture of two different siloxanes that were introduced on the surface of the nanoparticle.²³

Since the targeted protein has a similar size range as the nanoparticle, a surface fully covered with nickel would not be advantageous. Since the modified PEG chain (3) is longer than the unmodified chain, the nickel complex is still sterically accessible, which is crucial for an efficient interaction.²³

The successful introduction of the synthesized ligands onto the surface of the iron oxide nanoparticles (8.6 ± 0.6 nm, see Fig. S3†) was investigated with Fourier transform infrared spectroscopy (FTIR). Initially, the particles are coated with oleic acid, which is the ligand during their synthesis. It has some characteristic C–H vibrations at $2850\text{--}2920\text{ cm}^{-1}$ (see Fig. S4,† black curve), while the iron oxide core shows at 580 cm^{-1} .³⁸ After functionalization (see Fig. S4,† green curve), an ester peak becomes visible at 1740 cm^{-1} , caused by the three ester groups in the modified ligand; the iron oxide core is also clearly visible at 580 cm^{-1} . As stated in the experimental section, the *tert*-butyl groups of the ligand have to be removed before the modified nanoparticle is sufficiently water dispersible. After deprotection by trifluoroacetic acid (TFA), the ester group is replaced by a carboxylic acid, which can be seen in the FTIR spectra (see Fig. S5†).³⁵ TFA is the preferred deprotection agent since it does not dissolve the nanoparticle itself, as would hydrochloric acid.³⁵

If the deprotected IDA group is brought into contact with $\text{Ni}(\text{II})$ ions, a complex is formed as shown in Fig. 2. Investigating the presence of nickel atoms on the surface of the nanoparticles can be achieved by total reflection X-ray fluorescence (TXRF).

By adding an internal standard such as gallium, a concentration can be determined. The resulting spectrum is shown in the ESI (see Fig. S6†). After integration of the peaks, the nickel concentration was determined to $2.0\text{--}2.2\text{ mmol L}^{-1}$. Compared to iron from the core of the nanoparticle, the nickel/iron ratio is approximately 8–9%. This result can be expected since the core contains large amount of iron atoms and only a minor fraction (10%) of the ligands on the surface has affinity for nickel.

When these particles are dispersed in a cell lysate, they will interact specifically with the His-tagged proteins. Even though some proteins have histidine groups in their structure, their occurrence is low (2% of all protein residues).³⁹ Because some might have two or more adjacent histidine residues, a small amount of imidazole (10 mM) was added to one of the washing solutions. This strips off any loosely bound proteins, but is not high enough for release of the targeted protein. We preferred a His-tagged fluorescent protein (DsRed) as a model system, since it has a very characteristic absorbance spectrum, which greatly facilitates its detection and quantification.

After magnetic separation from the supernatant of the cell lysate, the particles are washed twice to remove all loosely (or nonspecifically) bound proteins from the surface. To release the His-tagged proteins, the particles are dispersed in a buffer with a high imidazole concentration (0.5 M). The particles were again magnetically separated, which yielded the elution fraction with the purified protein. A final wash step of the nanoparticles was performed to check if any proteins would be released. Fig. 3 shows the absorbance spectra of the supernatant (dashed) and elution fractions (solid). In the supernatant, no peak at 562 nm is visible, indicating a complete removal of the fluorescent protein. The background is caused by cellular debris and other proteins. The elution spectrum (after incubation with a high concentration of imidazole) however, clearly shows the characteristic peaks of DsRed. Hardly any proteins were found in the washing fractions (see Fig. S7†).

To investigate the purity of the obtained fractions, gel electrophoresis (SDS-PAGE) experiments were performed. As can be seen in Fig. 4, the supernatant has multiple bands, which correspond to cellular proteins. This result correlates well to the absorbance spectrum shown in Fig. 3.

The washing fractions show only a minor presence of DsRed proteins or cellular matrix proteins. This is a strong indication that aspecific adsorption on the iron oxide nanoparticles is minimal. The elution fraction on the other hand shows three bands that can be related to DsRed (compared to reference, final lane). No other bands are visible in the sample, which is good evidence that the obtained fluorescent proteins have a high purity. Finally, an extra washing step was performed, but there is only a very small presence of DsRed detectable. This gives a strong indication that the His-tagged proteins are efficiently stripped off the nanoparticles.

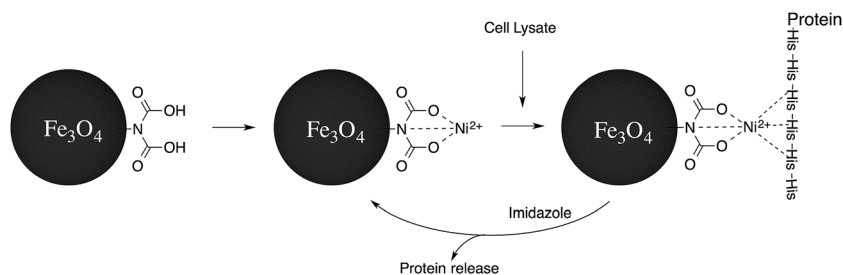


Fig. 2 After introduction of the ligand onto the nanoparticle's surface, it is loaded with nickel(II) ions. These interact with the His-tag of the proteins, which enables their magnetic separation. When imidazole is added, the proteins are released from the nanoparticles.

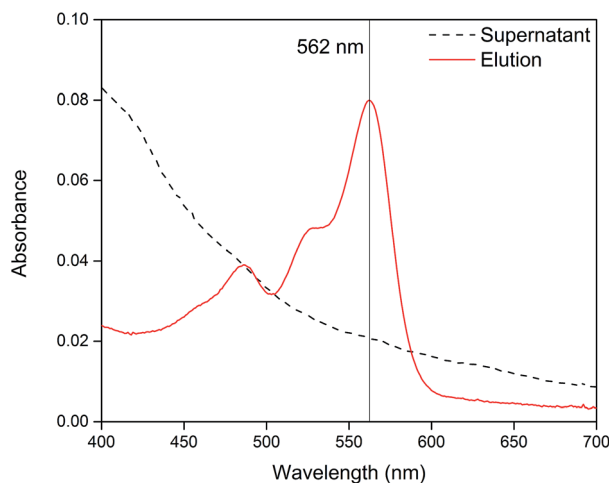


Fig. 3 The absorbance spectra of the supernatant and elution fractions show a clear difference. In the supernatant, no peaks (562 nm) of DsRed are visible, while the elution fraction shows a high signal. This illustrates the high efficiency of the magnetic capture and separation.

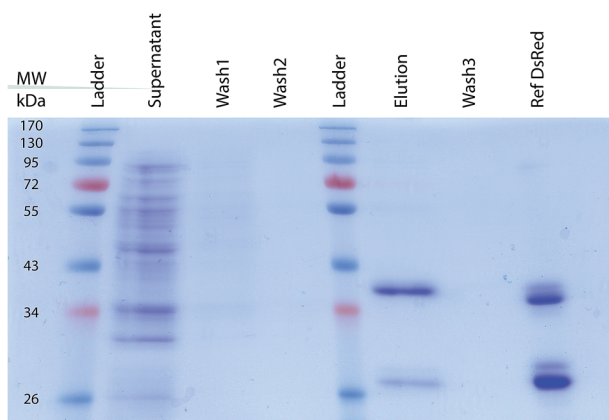


Fig. 4 Gel electrophoresis confirms that the purified DsRed fraction has a high purity. The supernatant contains multiple bands, corresponding to the cellular debris. The following washing steps show only minor bands, indicating that no proteins are being released from the nanoparticles at this stage. After contact with imidazole, the DsRed proteins are stripped off the nanoparticles (elution), resulting in two distinct bands in the gel, which correspond well with the reference (Ref DsRed). All bands are present in both samples, but since the concentration of the elution sample is lower, they are less pronounced.⁴⁰ The small shift (to lower mass) can be attributed to the shape of the gel, as can be seen when comparing both ladders. The final washing step (Wash3) shows no bands.

As stated before, the choice for IDA instead of NTA as the ligand for nickel might have consequences in terms of affinity for the metal ion. We investigated this by reusing the same batch of nanoparticles three times in similar purification experiments. Absorbance measurements and gel electrophoresis showed in this case that a decrease in efficiency could be observed (see Fig. S8 and S11[†]). The amount of targeted DsRed that remains in the supernatant increases, while the amount of recovered DsRed decreases. This is in accordance to the hypothesis that nickel atoms leach from the surface, decreasing

the general efficiency. However, a reloading step with nickel ions solves this issue (data in ESI, Fig. S9 and 10[†]).

Thanks to the magnetic properties and the large surface area of the nanoparticles, the entire purification process can be performed in less than 2 hours. Compared to the agarose-based method, which usually takes 4–5 hours, this is a great improvement. Moreover the magnetic approach is easily scalable and can be automated. Since the ligand is covalently bound and its concentration on the surface can be altered, a fully tailored nanoparticle surface can be obtained. This is a large advantage compared to polymer-coated particles, where the control over shell thickness and the amount of functional groups is limited. We therefore believe that the described methodology will be very valuable for future developments in selective magnetic purification.

Conclusions

Superparamagnetic iron oxide nanoparticles have tremendous potential for magnetic separation experiments. However their surface functionalization is crucial in this regard. We developed a heterobifunctional PEG ligand, with an IDA group on one end, which is capable of forming a complex with nickel ions. While on the other end, a siloxane was introduced that is capable of forming a covalent bond with an iron oxide surface, securing the ligands into place. This approach eliminates the chance of unwanted ligand exchange processes, while adding extra functionality. The IDA group was loaded with nickel(II) after which magnetic separation experiments of His-tagged fluorescent DsRed proteins from cell lysates were conducted. An efficient purification was observed, which was confirmed by absorbance measurements. Gel electrophoresis indicated that the obtained fluorescent proteins have a high purity. This approach can be highly valuable for the recuperation of tagged proteins from complex environments such as cell lysates, in a cost effective, time efficient manner.

Acknowledgements

The authors would like to thank prof. Johan Billen for helping with the TEM measurements. This work was financially supported by grants G.0618.11N and G.0484.12 of the Fund for scientific research Flanders (FWO-V) and the Agency for Innovation by Science and Technology in Flanders (IWT). M. Bloemen is grateful for support from the IWT.

References

- 1 A. S. Teja and P.-Y. Koh, *Prog. Cryst. Growth Charact. Mater.*, 2009, **55**, 22–45.
- 2 A. Ito, M. Shinkai, H. Honda and T. Kobayashi, *J. Biosci. Bioeng.*, 2005, **100**, 1–11.
- 3 J.-M. Montenegro, V. Grazu, A. Sukhanova, S. Agarwal, J. M. de la Fuente, I. Nabiev, A. Greiner and W. J. Parak, *Adv. Drug Delivery Rev.*, 2013, **65**, 677–688.
- 4 U. Jeong, X. Teng, Y. Wang, H. Yang and Y. Xia, *Adv. Mater.*, 2007, **19**, 33–60.

- 5 W. Brullot, R. Strobbe, M. Bynens, M. Bloemen, P.-J. Demeyer, W. Vanderlinden, S. de Feyter, V. K. Valev and T. Verbiest, *Mater. Lett.*, 2014, **118**, 99–102.
- 6 S. Carron, M. Bloemen, L. Vander Elst, S. Laurent, T. Verbiest and T. N. Parac-Vogt, *J. Mater. Chem. B*, 2015, **3**, 4370–4376.
- 7 Y. V. Kolen'ko, M. Bañobre-López, C. Rodríguez-Abreu, E. Carbó-Argibay, A. Sailsman, Y. Piñeiro-Redondo, M. F. Cerqueira, D. Y. Petrovykh, K. Kovnir, O. I. Lebedev and J. Rivas, *J. Phys. Chem. C*, 2014, **118**, 8691–8701.
- 8 D. Dupont, J. Luyten, M. Bloemen, T. Verbiest and K. Binnemans, *Ind. Eng. Chem. Res.*, 2014, **53**, 15222–15229.
- 9 M. Bloemen, C. Denis, M. Peeters, L. de Meester, A. Gils, N. Geukens and T. Verbiest, *Microchim. Acta*, 2015, **182**, 1439–1446.
- 10 J. Park, E. Lee, N.-M. Hwang, M. Kang, S. C. Kim, Y. Hwang, J.-G. Park, H.-J. Noh, J.-Y. Kim, J.-H. Park and T. Hyeon, *Angew. Chem., Int. Ed.*, 2005, **44**, 2873–2877.
- 11 J. Park, K. An, Y. Hwang, J.-G. Park, H.-J. Noh, J.-Y. Kim, J.-H. Park, N.-M. Hwang and T. Hyeon, *Nat. Mater.*, 2004, **3**, 891–895.
- 12 S. Laurent, D. Forge, M. Port, A. Roch, C. Robic, L. Vander Elst and R. N. R. N. Muller, *Chem. Rev.*, 2008, **108**, 2064–2110.
- 13 J. Sun, S. Zhou, P. Hou and Y. Yang, *J. Biomed. Mater. Res., Part A*, 2006, 333–341.
- 14 V. Vilas-Boas, N. Guldris, E. Carbó-Argibay, D. G. Stroppa, M. F. Cerqueira, B. Espiña, J. Rivas, C. Rodríguez-Abreu and Y. V. Kolen'ko, *RSC Adv.*, 2015, **5**, 47954–47958.
- 15 M. Bloemen, W. Brullot, T. T. Luong, N. Geukens, A. Gils and T. Verbiest, *J. Nanopart. Res.*, 2012, **14**, 1100–1109.
- 16 K. Turcheniuk, A. V. Tarasevych, V. P. Kukhar, R. Boukherroub and S. Szunerits, *Nanoscale*, 2013, **5**, 10729–10752.
- 17 E. Amstad, M. Textor and E. Reimhult, *Nanoscale*, 2011, **3**, 2819–2843.
- 18 D. Bhattacharya, S. K. Sahu, I. Banerjee, M. Das, D. Mishra, T. K. Maiti and P. Pramanik, *J. Nanopart. Res.*, 2011, **13**, 4173–4188.
- 19 J. A. Nye and J. T. Groves, *Langmuir*, 2008, **24**, 4145–4149.
- 20 D. C. Kaslow and J. Shiloach, *Nat. Biotechnol.*, 1994, **12**, 494–499.
- 21 G. S. Baird, D. A. Zacharias and R. Y. Tsien, *Proc. Natl. Acad. Sci. U. S. A.*, 2000, **97**, 11984–11989.
- 22 L. J. Gooßen and A. Döhring, *Synlett*, 2004, 0263–0266.
- 23 M. Bloemen, T. van Stappen, P. Willot, J. Lammertyn, G. Koeckelberghs, N. Geukens, A. Gils and T. Verbiest, *PLoS One*, 2014, **9**, e109475.
- 24 J. S. Kim, C. A. Valencia, R. Liu and W. Lin, *Bioconjugate Chem.*, 2007, **18**, 333–341.
- 25 Y. Zhang, Y. Yang, W. Ma, J. Guo, Y. Lin and C. Wang, *ACS Appl. Mater. Interfaces*, 2013, **5**, 2626–2633.
- 26 J. Cao, X. Zhang, X. He, L. Chen and Y. Zhang, *J. Mater. Chem. B*, 2013, **1**, 3625–3632.
- 27 W. Fang, X. Chen and N. Zheng, *J. Mater. Chem.*, 2010, **20**, 8624–8630.
- 28 D.-B. Shieh, C.-H. Su, F.-Y. Chang, Y.-N. Wu, W.-C. Su, J. R. Hwu, J.-H. Chen and C.-S. Yeh, *Nanotechnology*, 2006, **17**, 4174–4182.
- 29 S. K. Sahu, A. Chakrabarty, D. Bhattacharya, S. K. Ghosh and P. Pramanik, *J. Nanopart. Res.*, 2011, **13**, 2475–2484.
- 30 W. Wang, D. I. C. Wang and Z. Li, *Chem. Commun.*, 2011, **47**, 8115–8117.
- 31 G. Cheng, Z. G. Wang, Y. L. Liu, J. L. Zhang, D. H. Sun and J. Z. Ni, *ACS Appl. Mater. Interfaces*, 2013, **5**, 3182–3190.
- 32 G. Cheng, Y. Wang, Z.-G. Wang, X.-J. Sui, J.-L. Zhang and J.-Z. Ni, *RSC Adv.*, 2014, **4**, 7694–7702.
- 33 L. Gooßen and A. Döhring, *Adv. Synth. Catal.*, 2003, **345**, 943–947.
- 34 Y. E. Yan and F. W. Schwartz, *J. Contam. Hydrol.*, 1999, **37**, 343–365.
- 35 M. Bloemen, B. Sutens, W. Brullot, A. Gils, N. Geukens and T. Verbiest, *ChemPlusChem*, 2015, **80**, 50–53.
- 36 A. K. Tucker-Schwartz, R. A. Farrell and R. L. Garrell, *J. Am. Chem. Soc.*, 2011, **133**, 11026–11029.
- 37 C. E. Hoyle and C. N. Bowman, *Angew. Chem., Int. Ed.*, 2010, **49**, 1540–1573.
- 38 G. S. E. Antipas, E. Statharas, P. Tserotas, N. Papadopoulos and E. Hristoforou, *ChemPhysChem*, 2013, **14**, 1934–1942.
- 39 J. Bornhorst and J. Falke, *Methods Enzymol.*, 2000, **326**, 245–254.
- 40 A. Sacchetti, V. Subramaniam, T. M. Jovin and S. Alberti, *FEBS Lett.*, 2002, **525**, 13–19.